18TH WORLD CONFERENCE ON EARTHQUAKE ENGINEERING

WCEE2024

MILAN

MILAN, ITALY
30TH JUNE - 5TH JULY 2024

www.wcee2024.it

HIGH-FIDELITY MODELING OF FRACTURE-CRITICAL WELDED STEEL BEAM-TO-COLUMN CONNECTIONS

F. A. Galvis[1], G. G. Deierlein[2], C. Molina Hutt[3], & J. W. Baker[2]

[1] Thornton Tomasetti, San Francisco, United States, fgalvis@thorntontomasetti.com

[2] Stanford University, Stanford, United States

[3] The University of British-Columbia, Vancouver, Canada

Abstract: *Welded beam-to-column connections in steel moment frames built before the 1994 Northridge earthquake are susceptible to degradation triggered by fracture of the welded beam-to-column flange connection, followed by yielding and fracture of the bolted shear tab. Typical nonlinear frame analysis models used in design practice generally simulate these effects indirectly through phenomenological hinge-type models, which are computationally efficient but may not capture important response features. This paper describes a newly proposed nonlinear fiber-section model capable of explicitly simulating the degradation sequence of welded connections while maintaining the necessary computational efficiency for simulating overall building response. The proposed fiber section simulates weld fracture with a new SteelFractureDI material model that is implemented in OpenSees. This material model has a calibrated stress-based damage rule to predict fracture and crack closure under cyclic loading using 100 full-scale steel beam-to-column connection tests that failed due to flange fracture. The stress-based damage rule incorporates weld metal fracture toughness (Charpy-V-Notch energy) and weld flaw size to estimate the low-cycle fatigue fracture capacity of the welded flange joint. The proposed fiber-section approach overcomes the limitations of conventional concentrated plastic hinge models that simulate fracture with a constant rotation limit, which does not explicitly account for fracture behavior. The proposed connection model is employed in nonlinear dynamic analyses of two tall, welded steel moment frame building archetypes, and sensitivity analyses are performed to investigate the influence on the performance assessment of the connection model, uncertainty in fracture prediction, viscous damping parameters, and ground motion selection.*

1 Introduction

The skylines of major cities on the west coast of the United States are dominated by buildings that rely on older welded steel moment frames (WSMFs) for lateral load resistance (ATC-119 2018; Lai et al. 2015; Molina Hutt 2017). The 6.7 *Mw* Northridge (1994, California, US) and 6.9 *Mw* Kobe (1995, Japan) earthquakes demonstrated that WSMF buildings are prone to experiencing premature brittle fractures of beam-to-column joint welds under moderate to severe earthquake ground motions (Mahin 1998). Improving their inadequate performance can require complex retrofit interventions that are expensive and disruptive to building function; thus, motivating the need for rigorous performance-based assessments to quantify the building's earthquake risk and develop appropriate seismic retrofit options (ASCE/SEI 2017; NIST 2017a). The main tools to quantify risk and design retrofit interventions are detailed nonlinear response history analyses that capture all the relevant degradation mechanisms that may affect the structural response. In WSMFs, degradation often occurs in the beam-to-column connections and columns splices due to their high fracture vulnerability.

Fracture simulation in structural engineering generally uses one of three model types: (1) continuum Finite Element (FE), (2) Concentrated Plastic Hinges (CPH), or (3) distributed plasticity Fiber-Type models. Continuum FE models incorporate micromechanics and fracture theory to explicitly account for key factors in fracture prediction such as cyclic degradation of fracture strength, weld toughness, weld defects, and stress triaxiality (Chi et al. 2000; Goel et al. 1997; Kanvinde and Deierlein 2007; Matos and Dodds 2002; Ricles et al.

2000). However, these models require complex calibration, deep domain knowledge in fracture mechanics, and large computational resources to accurately simulate response for a connection subassembly. In contrast, CPH models are far more computationally efficient than FE models but sacrifice accuracy and precision. These models typically simulate fracture with a fixed connection rotation limit; thus, cyclic degradation of fracture strength, material toughness, weld defects, and stress triaxiality are not explicitly considered (NIST 2017b; c). This oversimplification results in the calibrated constant rotation limit having a large variance (FEMA 2000; Maison and Bonowitz 1999; NIST 2017b; c; Ramirez et al. 2012). Despite their limitations, CPH models are the current industry standard for modeling beam-to-column connections in WSMFs (ASCE/SEI 2017). Alternatively, fiber-type section models offer a compromise that balances the relative advantages and disadvantages of continuum FE and CPH models. Fiber-section models explicitly represent the geometry of structural members and material deterioration though unidirectional fiber models with appropriate kinematic constraints (e.g., plane sections remain plane) to simulate member behavior. Depending on the capabilities of the material models assigned to each fiber, a fiber-section approach avoids the oversimplification of CPH models while maintaining the computational efficiency necessary for analyzing entire buildings (NIST 2017d).

An additional challenge preventing reliable structural models of WSMFs is the significant number of assumptions required to idealize the structure and its earthquake hazard. These assumptions are often decided based on expert opinions since the literature lacks guidelines. For instance, the FEMA 355F (2000) state-of-the-art report lists recommendations for modeling beam-to-column connections, yet it does not include guidance for choosing the connection parameters nor does it account for their uncertainty. Consideration of uncertainties is also absent in the more recent ASCE/SEI 41 (2017) specification for seismic evaluation and retrofit of existing buildings. Similarly, the ground motions at a site could be selected and scaled using different spectral intensity targets, such as represented by the Uniform Hazard Spectrum (UHS), a conditional mean spectrum (Baker and Cornell 2006), or a conditional spectrum that includes the variability in shaking intensity (NIST 2011). Furthermore, one could impose further constraints on ground motion selection, including strong motion duration (Chandramohan et al. 2016a), velocity pulses (Orozco and Ashford 2002), or earthquake causal features, such as earthquake fault type, magnitude, distance to the building site, and site characteristics.

To address the aforementioned challenges, this paper presents the main features of a newly developed material model called *SteelFractureDI*, which the authors have implemented in OpenSees (McKenna 2011). Additionally, results of a sensitivity study are presented on the effect of the most common assumptions for modeling and selecting ground motions in collapse assessments of pre-Northridge tall WSMFs.

2   Connection behavior

To characterize the behavior of welded beam-to-column connections like those depicted in Fig. 1a, we compiled a database of 100 full-scale tests (Galvis et al. 2024b). This database includes pre- and post-Northridge connections tested in the past 60 years, including weak and strong panel zones as well as wide-flange and box column sections. This database also provides a digital twin for each test that enables the extraction of additional experimental information that was not collected during the test, such as the cyclic stress histories in the beam flanges.

This comprehensive database shows that the behavior of welded beam-to-column connections is controlled by two aspects of flange fracture. The first is the instant in the loading history when the first flange fractures. The second is the gapping behavior of fractured flanges observed when the crack closes during reverse loading.

The instant during the loading history when the first flange fractures produce three types of connection behaviors: Type 1 (Fig. 1b) connections that experience the first flange fracture while the connection remained entirely elastic, Type 2 (Fig. 1c) connections that experienced the first flange fracture after a very limited inelastic response, and Type 3 (Fig. 1d) connections that experienced the first flange fracture after a significant inelastic response. The force-displacement curves in Fig. 1b to Fig. 1d highlight the instant of flange fracture with a black circle and color-code the portion of the response that remained entirely elastic (blue), inelastic without fracture (red), and inelastic after fracture (green).

The experimental tests show that the immediate consequence of the first flange fracture is a large drop in force, and associated beam moment at the column face. Even after the first flange fractures, connections are still capable of resisting approximately 30% of their moment resistance through the force couple developed between tension resisted by the bolted shear tab and the opposing compression flange. Upon load reversal, the crack at the fractured flange closes and resists compression, while the opposing intact flange resists tension. Thus, the connection behaves as intact as long as the fractured flange crack is closed, and the other flange remains connected.
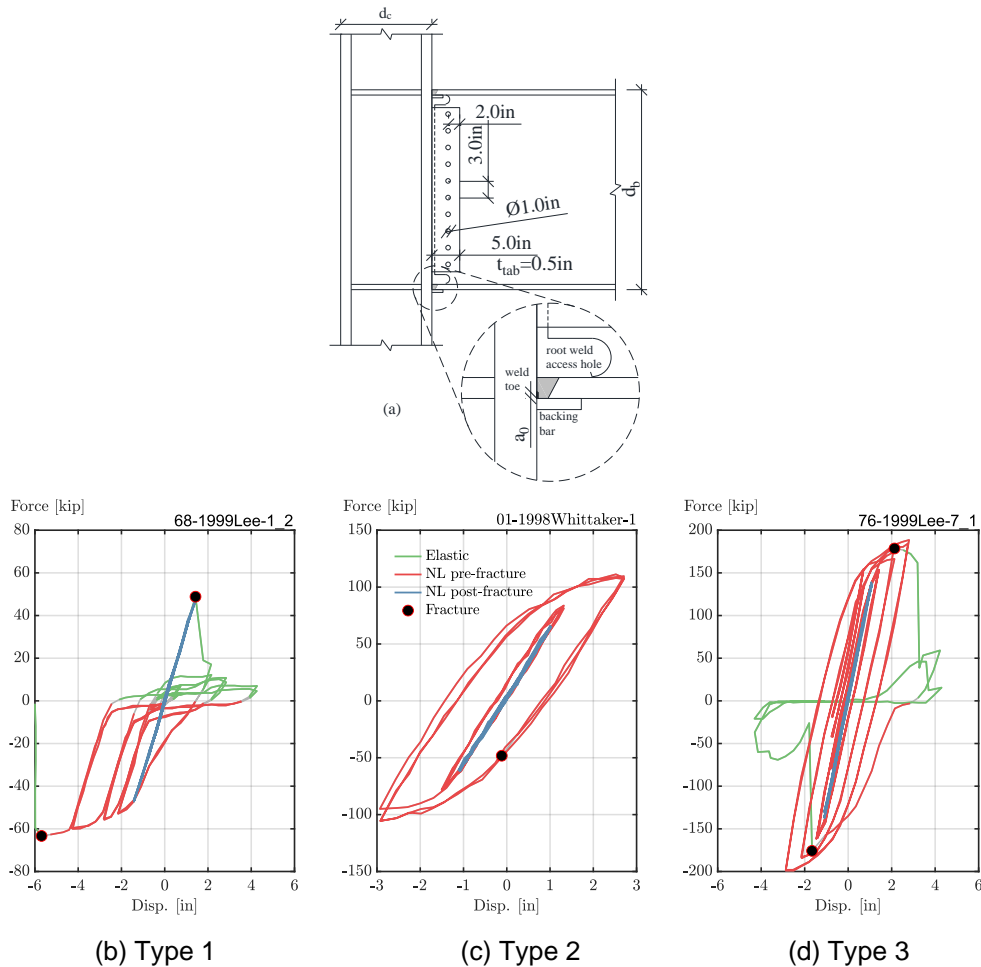
Figure 1. (a) Beam-to-column connection detail of pre-Northridge steel moment frames. Sample shear force-beam tip displacement response for connections behaviors (b) Type a, (c) Type 2, and (d) Type 3.

3   Proposed connection model

To efficiently capture the aforementioned behavior, we propose decoupling the fracture response model from one to capture other potential degradation mechanisms (e.g., local flange buckling) by using a fiber-section element in series with a ductile plastic hinge (Fig. 2a). Thus, complete connection model, which we implemented in OpenSees (McKenna 2011), combines (1) elastic elements with nonlinear springs to represent plastic hinging and degradation at the ends of the beams and columns, (2) Krawinkler's (1971) panel model, consisting of discrete rigid frame elements and a nonlinear spring (shown in yellow in Fig. 2a) to model inelastic panel zone response, and (3) a fiber-section element that simulates the welded flanges (shown with blue fibers) and the shear tab bolted connection (shown with red fibers). The flange fibers are assigned a newly proposed material constitutive model called *SteelFractureDI* to improve fracture prediction, allowing independent fracture of each flange and closely replicating the post-fracture connection behavior.

SteelFractureDI enables the explicit simulation of weld fracture and post-fracture crack closure to characterize response of the welded joints. This model predicts fracture based on a stress damage rule that simulates the evolving aspect of the fracture demand and capacity in real-time according to the fracture index, *FI*, given by Eq. 1. The *FI* model tracks the accumulation of damage based on cumulative tension and compressive stress

excursions, as compared to the fracture capacity, where fracture is triggered when *FI* = 1.0. An excursion refers to the total stress range between loading reversals. The fracture demand in the numerator of Eq. 1 is the difference between the tensile and compressive excursions. This coefficient β_c is less than 1, which implies an accumulation of damage under successive reverse cyclic loading.

$$FI = \frac{Cumm.\,tensile\,excursions \; - \; \beta_c \times Cumm.\,compressive\,excursions}{Fracture\,capacity} \qquad (1)$$

The fracture capacity corresponds to a critical stress value that is derived from fracture mechanics analyses to relate the flange stress to the critical stress intensity factor (K_{IC}), which accounts for weld metal fracture toughness (Charpy V-Notch, CVN, energy) and the weld defect size (a_0). The fracture capacity is calculated by Eq. 2 and 3 for a top or bottom welded detail, respectively. The coefficient *k* in these equations capture additional aspects of the connection that influence the fracture capacity such as panel zone strength ratio and flange thickness. Eq. 3 and 4 are an adaptation of the definition of critical stress presented in NIST (2017c), which is based on previous fracture mechanics studies of welded connections (Chi 1999; Stillmaker 2016). To calibrate these equations, we compiled a complementary database of CVN and a_0 from published reports of damaged building after the 1994 Northridge earthquake and full-scale tests. This data shows that the median CVN and a_0 for pre-Northridge welded flanges is 12 ft-lb and 0.12 times the flange thickness (t_f), respectively.

$$Fracture\,capacity_{bottom} = k\,\frac{K_{IC}(CVN)}{1.2 + 2a_0} \qquad (2)$$

$$Fracture\,capacity_{top} = k\,\frac{K_{IC}(CVN)}{0.5 + 2a_0} \qquad (3)$$

The behavior of the *FI* is illustrated in Fig. 2b with an example beam-to-column connection subjected to cyclic loading. These parameters were calibrated to ensure that *FI*=1.0 at the instant of flange fracture. The *FI* function shows a monotonic increasing trend representing the damage caused by successive tensile and compressive excursion. The higher-frequency spikes correspond to the recoverable damage when the stress reverses. More details on the fracture index formulation and parameter calibration based on the 100 test connection database can be found in Galvis et al. (2024a). Owing to the inherent variability in the fracture response, the *FI* is statistically related to the experimental data through a Weibull distribution with median value of *FI* =1.0 and a coefficient of variation of 0.24 for the bottom flange and 0.22 for the top flange (Galvis et al. 2024a).
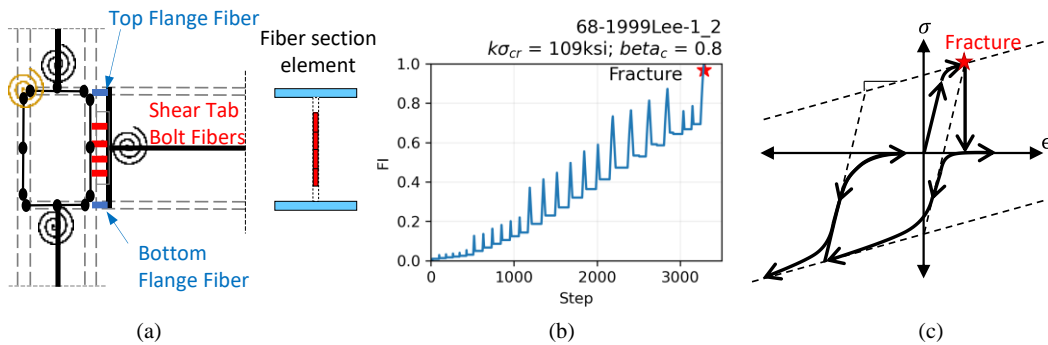
Figure 2: (a) Schematic depiction of the fiber-section model for welded-flange and bolted web connections. (b) Sample evolution of the real-time Fracture Index (FI) on a cyclic beam-to-column connection test. (c) Post-fracture constitutive law for the flange fiber materials to simulate the opening and closing of the crack.

As illustrated schematically in Fig. 2c, the resulting *SteelFractureDI* captures the full range of response of the welded joint. Flange tensile stress is released when the computed *FI* reaches its critical value, based on the Weibull distribution that has been calibrated to past connection tests. Subsequent crack closure is modeled by a gradually increasing resistance of compressive (negative) stress following a smooth curve for numerical stability. The example in Fig. 2c shows that the strain increases toward negative values to yield the material in compression to then reverse again dropping the stress to zero (crack opening). This weld material model considers the last unloading cycle to update the location of the fractured surface and pick up compressive stresses at the appropriate location of crack closure.

4   Building archetypes

To evaluate the impacts of the proposed connection model and draw practical recommendations for structural engineers interested in quantifying the stability against collapse of WSMFs, we performed a sensitivity study with the two frame archetypes shown in Fig. 3a and Fig. 3b. These archetypes are inspired by existing buildings in San Francisco and are generally representative of frame designs of the late-1960s through mid-1970s. Both archetypes comply with the applicable building code in effect at the time of their design, representing space frame configurations of similar age and height, but with different dynamic properties. Based on the calculated building periods, building A (Fig. 3a) is a significantly more flexible system than building B (Fig. 3b), because building A has both proportionally smaller section sizes and fewer framing bays than building B.

Year	1971
No. stories	42
Height	474 ft
No. bays	3
Frame	Space
T_1	5.00 s
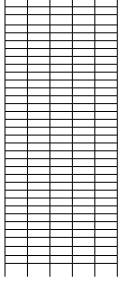
Year	1971
No. stories	35
Height	472 ft
No. bays	5
Frame	Space
T_1	3.70 s

(a)   (b)

Figure 3: Tall building archetypes of similar completion year and height: (a) building A (flexible archetype) and (b) building B (stiff archetype).

5   Sensitivity study methodology

There are four classifications of important assumptions for modeling WSMFs:

1.   Selecting the connection model and weld properties (e.g., CVN and a0).
2.   Accounting for uncertainties in fracture prediction.
3.   Selecting a damping model.
4.   Defining the criteria for ground motion selection.

In this study, we performed a simple sensitivity study on all the aforementioned assumptions to quantify their impact on the risk of building collapse. To this end, we developed a baseline model for both building archetypes and a series of variations to that baseline that enable isolating the effects of each modeling assumption.

5.1 Collapse analysis methodology

Collapse risk is measured in terms of the probability of collapse in 50 years, $P_c^{50\ years}$, which combines the vulnerability of the structure with the seismic hazard at the site across all possible ground motion intensities. This metric assumes that collapse occurrence follows the exponential distribution presented in Eq. 4 (Baker et al. 2021), where λ_c is the mean annual frequency of collapse, which is calculated with the convolution integral of Eq. 5. This equation integrates the product of the collapse fragility of the structure, $P(C|IM)$, and the slope of the seismic hazard curve, $\left|\frac{d\lambda_{im}}{dIM}\right|$ over all the possible ground motion intensities (*IM*).

$$P_c^{50\ years} =\ 1 - \exp(-50\lambda_c) \tag{4}$$

$$\lambda_c =\ \int_0^\infty P(C|IM)\left|\frac{d\lambda_{im}}{dIM}\right|dIM \tag{5}$$

The $P(C|IM)$ is assumed to be a lognormal cumulative distribution, whose parameters are estimated with maximum likelihood for each building model (Baker 2015) using the results of a multi-stripe analysis, MSA (Jalayer 2003). The method is called, 'multi-stripe' since it involves the calculation of 'stripes' of structural response data at several discrete ground motion intensities. In this study, the MSA is used to estimate the fraction of building collapses from sets of ground motions at increasing levels of intensity. The MSA is performed in the following three steps for each discrete ground motion intensity: (1) select a set of ground motion time histories following specific criteria that aligns with general guidelines prescribed in building codes, (2) analyze the building for each ground motion in the set to determine whether the building collapses or

survives the motion, and (3) compute the fraction of collapses at each stripe by dividing the number of ground motions that caused collapse over the total number of ground motions in the set.

5.2 Baseline structural modeling

The baseline building model has a connection modeled with fiber-section elements with assumed weld properties of CVN=12 ft-lb and a_0=0.1t_f (t_f, beam flange thickness). These parameters represent the median CVN and a_0 collected from damaged buildings after the 1994 Northridge earthquake. In the baseline case, connection model uncertainty is ignored, so CVN, a_0, and the critical *FI* are the same for all the connections in the building (except to the extent that t_f varies with beam sizes). Viscous damping is modeled using the Rayleigh formulation with 2% critical damping at periods corresponding to the vibration modes 1 and 3. The ground motions were selected using conditional spectra (Baker and Lee 2018) for a site in downtown San Francisco, with conditioning periods equal to the fundamental period (3.7s and 5.0s) of each building.

5.2. Building model variations

For the sensitivity study, we created 13 variations of the baseline model, as summarized in Table 1. Models 1 and 2 use a plastic-hinge type connection model with properties based on ASCE 41-17 for pre- and post-Northridge connection details. Models 3 and 4 use the proposed fiber-type connection model (same as the baseline), but with higher CVN weld material toughness. Models 5 to 7 incorporate modeling uncertainty in fracture prediction, where: Model 5 is identical to the baseline model but injects the uncertainty in *FI* by sampling the critical *FI* for each connection from a Weibull distribution; and Models 6 and 7 consider the uncertainty in *FI* in addition to variability in the distribution of CVN values in the building. Model 6 uses one unique CVN realization for the entire building at each ground motion, and Model 7 samples independently the CVN for each connection and ground motion. The CVN values are sampled from a lognormal distribution with a 12ft-lb median and 0.2 coefficient of variation. Models 8 to 10 vary the assumed viscous damping coefficients. Model 8 uses a high specified damping ratio from (of 5%), while models 9 and 10 maintain the baseline damping ratio of 2% but vary the anchoring periods. Finally, models 11 and 12 are run with alternate ground motion sets, which are described in Section 6.

Table 1: List of variations to the model baseline considered in the sensitivity analysis.

Building	Modeling assumption	Ground motion set	$P_c^{50years}$
A	0. Baseline	CS $T_{cond} = T_1$	0.15
	1. Connections ASCE Pre-NR	"	0.13
	2. Connections ASCE Post-NR	"	0.06
	3. Connections CVN = 20ft-lb	"	0.09
	4. Connections CVN = 40ft-lb	"	0.07
	5. Uncertainty in FI	"	0.13
	6. Uncertainty in FI and CVN (Uniform)	"	0.15
	7. Uncertainty in FI and CVN (by connection)	"	0.13
	8. 5% Rayleigh damping at T1 and T3	"	0.13
	9. 2% Rayleigh damping at T1 and T10	"	0.16
	10. 2% Rayleigh damping at T1/2 and T3	"	0.15
	11. Baseline	CS T_{cond} = 1.0s	0.17
	12. Baseline	UHS	0.16
	13. Baseline	CS T_{cond} = T_1 & Long D_{s575}	0.18
B	0. Baseline	CS T_{cond} = T_1	0.055
	1. Connections ASCE Pre-NR	"	0.027
	2. Connections ASCE Post-NR	"	0.014
	3. Connections CVN = 20ft-lb	"	0.030
	4. Connections CVN = 40ft-lb	"	0.021
	5. Uncertainty in FI	"	0.060
	6. Uncertainty in FI and CVN (Uniform)	"	0.050
	7. Uncertainty in FI and CVN (by connection)	"	0.058
	8. 5% Rayleigh damping at T1 and T3	"	0.036
	9. 2% Rayleigh damping at T1 and T10	"	0.055
	10. 2% Rayleigh damping at T1/2 and T3	"	0.055
	11. Baseline	CS T_{cond} = 1.0s	0.052
	12. Baseline	UHS	0.075
	13. Baseline	CS T_{cond} = T_1 & Long D_{s575}	0.084

6   Ground motion sets

The sensitivity study evaluates the effect of three assumptions in ground motion selection: the target spectra, the conditioning period, and strong-motion duration. To this end, we selected sets of 70 ground motions at six intensities with the following return periods: 72, 140, 225, 475, 975, and 2475 years.

The four different ground motion selection targets are: (1) conditional spectra at the fundamental period of the building (CS $T_{cond}=T_1$), (2) conditional spectra at 1.0s to capture higher-mode effects (CS $T_{cond}=1.0s$), (3) uniform hazard spectra (UHS), and (4) spectrally equivalent long duration sets conditioned on the fundamental period of the building (CS $T_{cond}=T_1$ & Ds5-75). The ground motion duration is defined in terms of 5-75% significant duration (D_{s5-75}), where the spectrally equivalent long-duration sets have duration distribution that are based on sites, such as Eugene, OR, where the hazard is dominated by subduction interface earthquakes (with D_{s5-75} between 30 and 50s). The baseline case assumes that the sets have durations similar to those expected in San Francisco (with D_{s5-75} between 10s and 30s). For further information on the definition and effects of ground motion duration, see (Chandramohan et al. 2016b)
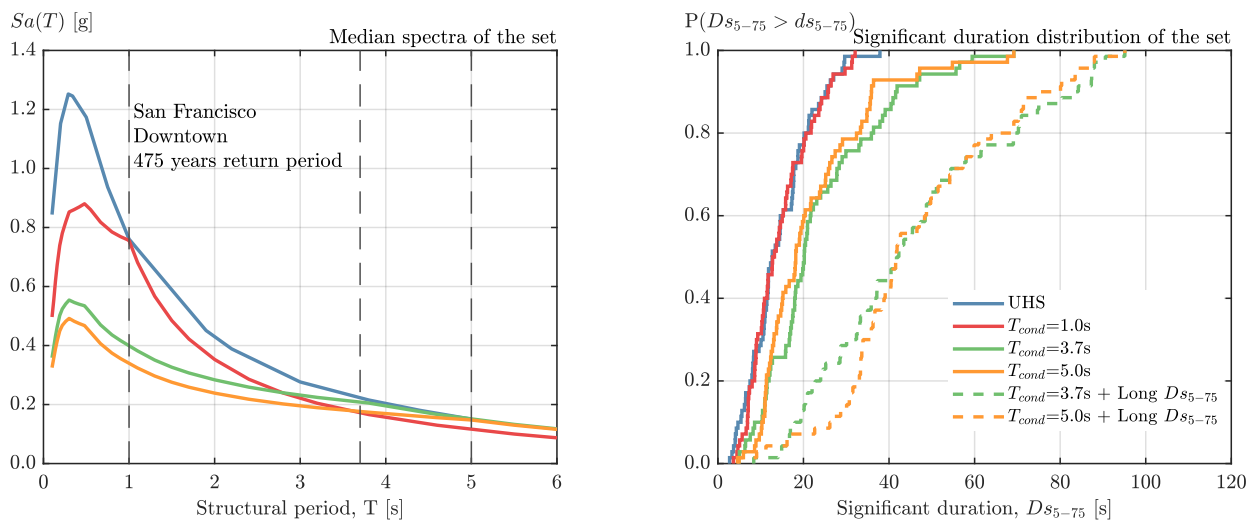
Figure 4: Ground motion set characteristics for the sets selected to represent the 475-year intensity. (a) Target pseudo-acceleration spectra; and (d) significant duration distribution of the selected set.

The median spectra of the ground motion sets, selected for the 475-year return period, are shown in Fig. 4a. By definition, the UHS spectrum represents the largest intensities at every period while the other spectra consider a more realistic spectral shape conditioning in different periods. Fig. 4b shows the corresponding distribution of the significant duration for the 475-year return period sets. Except for the one long-duration set, ground-motion duration was not explicitly considered in the record selection, and the resulting durations generally reflect the prevalence of moderate magnitude earthquake records (Moment Magnitude = 5 to 7) in available ground motion databases. This approach yielded very similar duration distributions for the UHS and CS $T_{cond}=1.0s$ sets and a slightly longer duration for the CS sets conditioned to 3.7s and 5.0s.

7   Implications on collapse stability

This section summarizes the results and implications on collapse risk of the four groups of modeling assumptions considered in the sensitivity study. The $P_c^{50\ years}$ for each model are listed in the last column of Table 1. For buildings A and B respectively, the baseline model using the CS $T_{cond} = T_1$ ground motion set has a $P_c^{50\ years}$ equal to 0.15 and 0.04. The calculated collapse risks are significantly larger than the $P_c^{50\ years}$ value of 0.01 assumed in developing the risk-targeted MCEr maps of ASCE 7(Luco et al. 2007).

7.1 Connection model and weld material properties

The collapse fragilities of each archetype using different connection models is presented in Fig. 5. To ease comparison between the archetypes with different fundamental periods, we normalized the horizontal axis of the collapse fragilities by the corresponding intensity at MCEr from the ASCE 7-16 design code at the site. These fragility functions show the drastically different behavior of these two archetypes where building A is significantly more vulnerable than building B. This difference in collapse safety of the buildings is evident in

the distinct collapse mechanisms depicted in Fig. 5 for each frame. The collapse behavior of building A is dominated by a single collapse mechanism driven by P-Delta effects due to the lower stiffness of the frame. The collapse modes of building B, however, are more sensitive to the distribution of connection fractures whose locations are more varied.
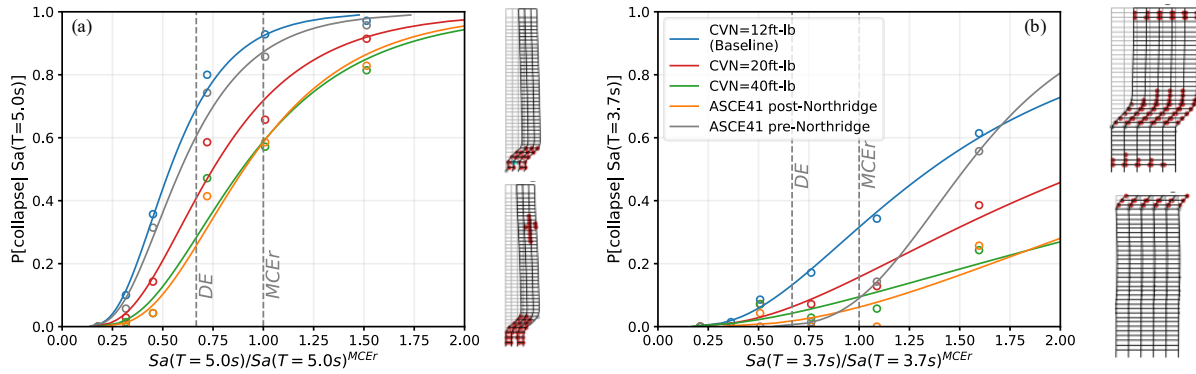
Figure 5: Collapse fragility functions varying the connection model and fracture toughness for frames (a) building A and (b) building B.
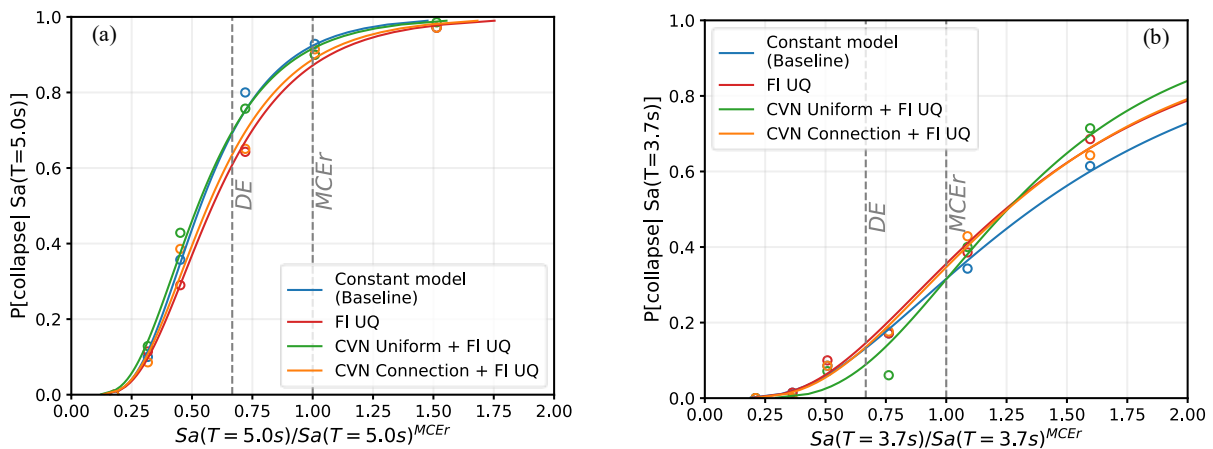
Figure 6: Collapse fragility functions varying the assumptions on fracture uncertainty propagation for frames (a) building A and (b) building B.

The collapse fragilities in Fig. 5 show that the connection model tremendously impacts the resultant collapse fragility. The baseline model using the proposed fiber section has a larger collapse probability for all the intensities compared to the ASCE41 pre-Northridge model, suggesting a potential unconservative bias in the ASCE41 connection model. This difference is more pronounced in building B, which is more sensitive than building A to individual connection fractures. Increasing the CVN shifts the fragility function to the right in both buildings, causing large reductions in the collapse probability. Assuming a CVN=40ft-lb prevents almost any connection fracture and the performance of the building approaches the collapse fragility of the model using ductile plastic hinges (ASCE 41 post-Northridge). This sensitivity to the connection model highlights the significance of this work to quantify actual risk in buildings if CVN samples are obtained.

7.2 Uncertainty in fracture prediction

The collapse fragilities of both archetypes are mostly insensitive to the uncertainty in fracture prediction (Fig. 6). Note that despite the fragilities being very similar, individual structural analysis and damage distributions differ between models with or without fracture uncertainty since the fraction of collapses changes for each model at the same stripe. This change of collapse fraction means that the uncertainty in fracture prediction may be ignored as long as the engineer is interested in overall safety metrics rather than structural response to a specific ground motion.

8

7.3 Damping model selection

Similar to the uncertainty in fracture prediction, the choice of viscous damping parameters (i.e. damping ratio and anchor periods) have little impact on the resultant collapse fragility function (Fig. 7). This conclusion holds true for the two extreme choices of anchored periods in both buildings. Nevertheless, increasing the damping ratio from 2% to 5% causes a moderate reduction of the collapse probabilities for building B.
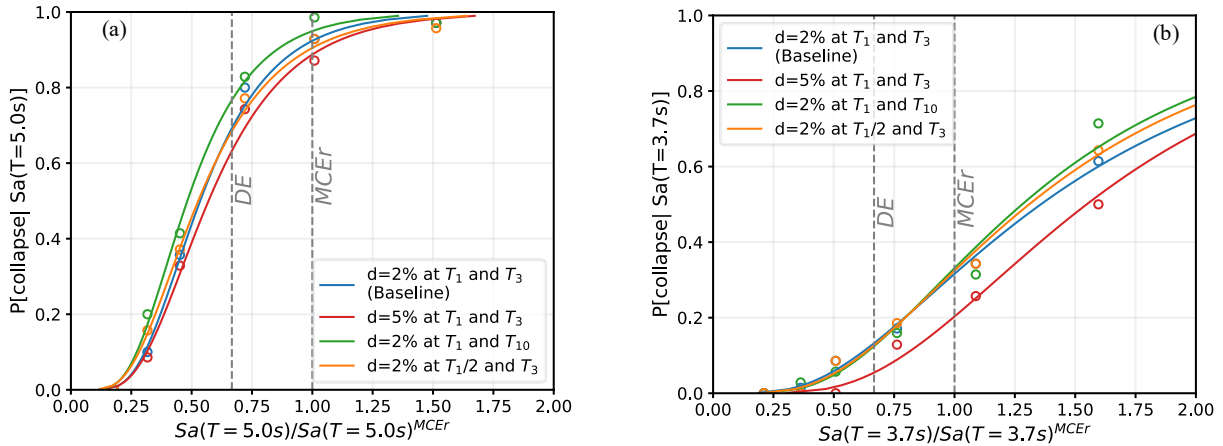
Figure 7: Collapse fragility functions varying the assumptions on the damping model for frames (a) building A and (b) building B.
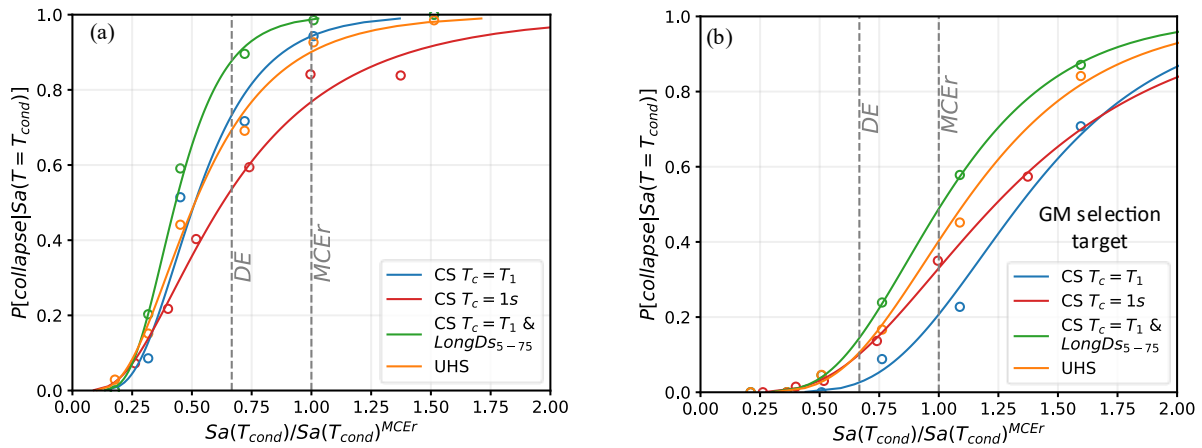
Figure 8: Collapse fragility functions varying the ground motions selection parameters and most common collapse mechanisms for frames (a) building A and (b) building B.

7.4 Ground motion characteristics

The four ground motion sets described in Section 6 noticeably change the resultant collapse fragility as depicted in Fig. 8. Since the response of building A is dominated by overall flexibility, the resultant collapse fragilities calculated using the four ground motion sets are very similar in the lower tail of the distribution (Fig. 8a). In contrast, the fragilities vary at higher intensities, where the CS T_{cond}=1.0s ground motion set yields the lowest collapse risk, while the long duration set (CS T_{cond} =T_1 & Ds5-75) yields the highest risk. By contrast, building B experiences a shift in the median collapse capacity with each ground motion selection criterion, indicating that the selection targets are more important for buildings that experience more varied collapse mechanisms under different earthquake input motions.

Modeling the welded connections with a fiber section using *SteelFractureDI* uncovers the significant impact of ground motion duration on the risk of WSMFs as depicted by the difference in the collapse fragilities for spectrally equivalent record sets (blue and green in Fig. 8). Longer ground motions are more detrimental to

welded connections than shorter motions because the additional number of cycles further reduces the fracture capacity of the connections. Typical hinge models that use constant rotation limits to simulate fracture ignore this cyclic aspect of the behavior and fail to the capture this fundamental degradation mechanism.

7.5 Summary results from the sensitivity analysis

The results of the sensitivity study are summarized in Fig. 9 and Fig. 10, which presents the probability of collapse in 50 years for the models of building A and B, respectively. The baseline collapse risk is denoted with a horizontal dashed line. This figure shows that the connection model is the most important decision for estimating the collapse risk of steel frames followed by the ground motion selection criteria. These results underscore the importance of ground motion duration and suggest that, in some instances, duration is as important as spectral shape. Moreover, ignoring the uncertainty in fracture prediction and viscous damping parameters may be an acceptable modeling practice.
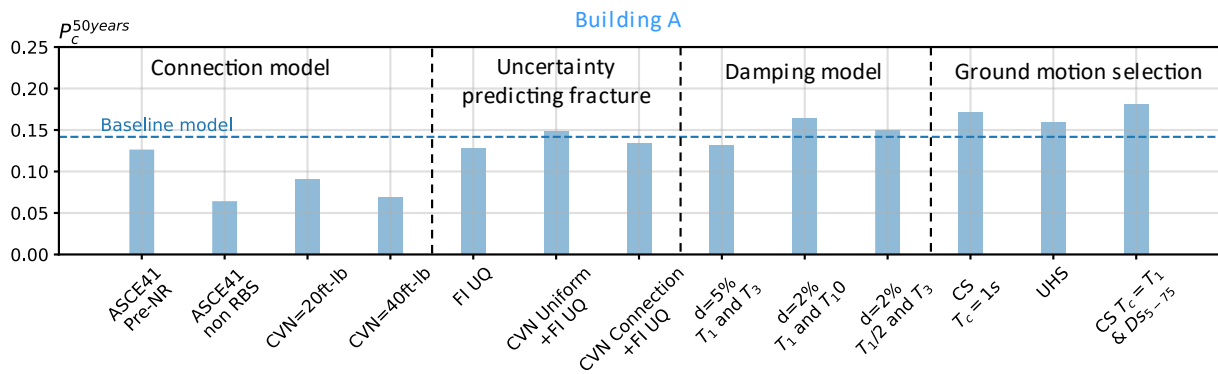
Figure 9: Summary of the collapse risk for Building A
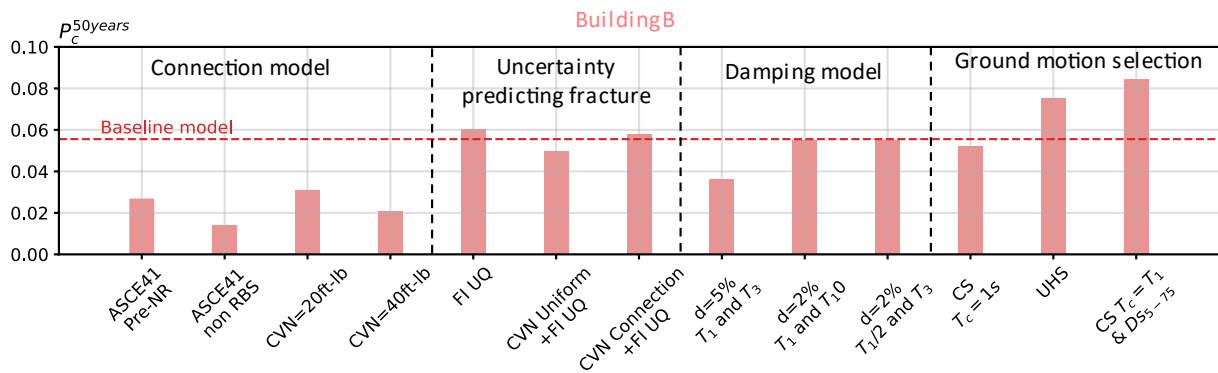
Figure 10: Summary of the collapse risk for Building B

8   Conclusions

This paper summarizes the application of a high-fidelity model to simulate earthquake response of steel buildings with fracture-vulnerable welded connections. The key contribution of this work is the development of a novel material model implemented in OpenSees called *SteelFractureDI*. This model allows an efficient and yet accurate prediction of fracture by explicitly considering the measured toughness and flaw size of welded flanges in beam-to-column connections. *SteelFractureDI* is also equipped with a new post-fracture constitutive law that simulates full response of fractured flanges that are incapable of transmitting tensile stresses but could transfer compression when the crack closes in reverse loading.

We applied the proposed connection model to two representative tall buildings located in downtown San Francisco, and we performed a sensitivity study to develop practical guidelines for structural modeling geared towards collapse risk quantification. The study focused on four assumptions that are subjectively selected in conventional practice: (1) choice of the connection model and median material properties; (2) handling of modeling uncertainty in the connection modeling; (3) viscous damping model parameters; and (4) ground motion selection criteria. The results show that the connection model and median material properties are

critical decisions that have a large impact in the resultant risk. In contrast, explicit quantification of the uncertainty in fracture prediction and damping model parameters only negligibly affect the building's risk.

Ground motion selection criteria are as important as selecting the proper connection model for well-proportioned frames that are sensitive to the number and locations of fractured connections. Moreover, these results provide evidence that ground motion duration is as important as spectral shape when estimating the risk of steel buildings using high-fidelity models that capture low-cycle fatigue demands. However, the ground motion selection is less relevant for very flexible frames with dynamic instability driven by P-Delta effects.

9   Acknowledgments

10 References

ASCE/SEI. (2017). *Seismic Evaluation and Retrofit of Existing Buildings (ASCE/SEI 41-17)*. Reston, Virginia.

ATC-119. (2018). *San Francisco Tall Buildings Study*. Redwood City, CA.

Baker, J. W. (2015). "Efficient analytical fragility function fitting using dynamic structural analysis." *Earthquake Spectra*, 31(1), 579–599.

Baker, J. W., Bradley, B. A., and Stafford, P. J. (2021). *Seismic Hazard and Risk Analysis*. Cambridge University Press, Cambridge, England.

Baker, J. W., and Cornell, A. C. (2006). "Spectral shape, epsilon and record selection." *Earthquake Engineering and Structural Dynamics*, 35(9), 1077–1095.

Baker, J. W., and Lee, C. (2018). "An Improved Algorithm for Selecting Ground Motions to Match a Conditional Spectrum." *Journal of Earthquake Engineering*, Taylor & Francis, 22(4), 708–723.

Chandramohan, R., Baker, J. W., and Deierlein, G. G. (2016a). "Quantifying the influence of ground motion duration on structural collapse capacity using spectrally equivalent records." *Earthquake Spectra*, 32(2), 927–950.

Chandramohan, R., Baker, J. W., and Deierlein, G. G. (2016b). "Impact of hazard-consistent ground motion duration in structural collapse risk assessment." *Earthquake Engineering & Structural Dynamics*, 45(8), 1357–1379.

Chi, W.-M. (1999). "Prediction of Steel Connection Failure Using Computational Fracture Mechanics." Stanford University.

Chi, W.-M., Deierlein, G. G., and Ingraffea, A. (2000). "Fracture Toughness Demands in Welded Beam-Column Moment Connections." *Journal of Structural Engineering*, 126(1), 88–97.

Fema-355F. (2000). "State of the Art Report on Performance Prediction and Evaluation of Steel Moment-Frame Buildings."

FEMA. (2000). "FEMA 355F State of the Art Report on Performance Prediction and Evaluation of Steel Moment-Frame Buildings."

Galvis, F. A., Deierlein, G. G., Yen, W., and Molina Hutt, C. (2024a). "Fracture-Mechanics Based Material Model for Fiber Simulation of Weld Fractures in Steel Moment Frames." *(In preparation)*.

Galvis, F. A., Deierlein, G. G., Yen, W., Molina Hutt, C., and Correal, J. F. (2024b). "Database of Fracture Critical Steel Beam-to-Column Connections Augmented with Digital Twins." *Journal of Structural Engineering (In Press)*.

Goel, S. C., Stojadinović, B., and Lee, K. (1997). "Truss analogy for steel moment connections." *Engineering Journal*, 2, 43–53.

Jalayer, F. (2003). "Direct Probabilistic Seismic Analysis : Implementing Non-Linear Dynamic Assessments." Stanford University.

Kanvinde, A., and Deierlein, G. G. (2007). "Cyclic Void Growth Model to Assess Ductile Fracture Initiation in Structural Steels due to Ultra Low Cycle Fatigue." *Journal of Engineering Mechanics*, 133(6), 701–712.

Krawinkler, H. (1971). *Inelastic behavior of beam-column subassemblies (Report EERC-71-07)*. Earthquake Engineering Research Center, Berkeley, California.

Lai, J.-W., Wang, S., Schoettler, M. J., and Mahin, S. A. (2015). "PEER Seismic Evaluation and Retrofit of Existing Tall Buildings in California." *PEER Report No. 2015/14*.

Luco, N., Ellingwood, B. R., Hamburger, R. O., Hooper, J. D., Kimball, J. K., and Kircher, C. a. (2007). "Risk-targeted versus current seismic design maps for the conterminous united states." *Structural Engineering Association of California 2007 Convention Proceedings*, 1–13.

Mahin, S. A. (1998). "Lessons from damage to steel buildings during the Northridge earthquake." *Engineering Structures*, 20(4–6), 261–270.

Maison, B. F., and Bonowitz, D. (1999). "How Safe Are Pre-Northridge WSMFs? A Case Study of the SAC Los Angeles Nine-Story Building." *Earthquake Spectra*, 15(4), 765–789.

Matos, C. G., and Dodds, R. H. (2002). "Probabilistic modeling of weld fracture in steel frame connections Part I: quasi-static loading." *Engineering Structures*, 24(6), 687–705.

McKenna, F. (2011). "OpenSees: A framework for earthquake engineering simulation." *Computing in Science and Engineering*, IEEE, 13(4), 58–66.

Molina Hutt, C. (2017). "Risk-Based Seismic Performance Assessment of Existing Tall Steel Framed Buildings."

NIST. (2011). *Selecting and Scaling Earthquake Ground Motions for Performing Response-History Analyses. NNIST GCR 11-917-15*, Washington, DC.

NIST. (2017a). "Guidelines for nonlinear structural analysis and design of buildings. Part I - general." *NIST GCR 17-917-46v1*.

NIST. (2017b). *Recommended modeling parameters and acceptance criteria for nonlinear analysis in support of seismic evaluation, retrofit, and design. NIST GCR 17-917-45*.

NIST. (2017c). "Guidelines for Nonlinear Structural Analysis for Design of Buildings Part IIa-Steel Moment Frames." *NIST GCR 17-917-46v2*.

NIST. (2017d). *Guidelines for Nonlinear Structural Analysis for Design of Buildings Part I-General Applied Technology Council. NIST GCR 17-917-46v1*.

Orozco, G. L., and Ashford, S. a. (2002). *Effects of Large Velocity Pulses on Reinforced Concrete Bridge Columns Concrete Bridge Columns. Pacific Earthquake Engineering Research Center*.

Ramirez, C. M., Lignos, D. G., Miranda, E., and Kolios, D. (2012). "Fragility functions for pre-Northridge welded steel moment-resisting beam-to-column connections." *Engineering Structures*, 45, 574–584.

Ricles, J. M., Mao, C., Lu, L.-W., and Fisher, J. W. (2000). *Development and Evaluation of Improved Details for Ductile Welded Unreinforced Flange Connections (SAC_BD-00_24)*. Sacramento, California.

Stillmaker, K. R. (2016). "Probabilistic Fracture Mechanics Based Assessment of Welded Column Splices in Steel Moment Frames By Approved :"